



Article

Crystal Chemistry of Stanfieldite, $\text{Ca}_7\text{M}_2\text{Mg}_9(\text{PO}_4)_{12}$ ($M = \text{Ca}, \text{Mg}, \text{Fe}^{2+}$), a Structural Base of $\text{Ca}_3\text{Mg}_3(\text{PO}_4)_4$ Phosphors

Sergey N. Britvin ^{1,2,*} , Maria G. Krzhizhanovskaya ¹, Vladimir N. Bocharov ³  and Edita V. Obolonskaya ⁴

¹ Department of Crystallography, Institute of Earth Sciences, St. Petersburg State University, Universitetskaya Nab. 7/9, 199034 St. Petersburg, Russia; mariya.krzhizhanovskaya@spbu.ru

² Nanomaterials Research Center, Kola Science Center of Russian Academy of Sciences, Fersman Str. 14, 184209 Apatity, Russia

³ Centre for Geo-Environmental Research and Modelling, Saint-Petersburg State University, Ulyanovskaya ul. 1, 198504 St. Petersburg, Russia; bocharov@mosp.phys.spbu.ru

⁴ The Mining Museum, Saint Petersburg Mining University, 2, 21st Line, 199106 St. Petersburg, Russia; musmet11@yandex.ru

* Correspondence: sergei.britvin@spbu.ru

Received: 1 May 2020; Accepted: 25 May 2020; Published: 1 June 2020



Abstract: Stanfieldite, natural Ca-Mg-phosphate, is a typical constituent of phosphate-phosphide assemblages in pallasite and mesosiderite meteorites. The synthetic analogue of stanfieldite is used as a crystal matrix of luminophores and frequently encountered in phosphate bioceramics. However, the crystal structure of natural stanfieldite has never been reported in detail, and the data available so far relate to its synthetic counterpart. We herein provide the results of a study of stanfieldite from the Brahin meteorite (main group pallasite). The empirical formula of the mineral is $\text{Ca}_{8.04}\text{Mg}_{9.25}\text{Fe}_{0.72}\text{Mn}_{0.07}\text{P}_{11.97}\text{O}_{48}$. Its crystal structure has been solved and refined to $R_1 = 0.034$. Stanfieldite from Brahin is monoclinic, $C2/c$, a 22.7973(4), b 9.9833(2), c 17.0522(3) Å, β 99.954(2)°, V 3822.5(1) Å³. The general formula of the mineral can be expressed as $\text{Ca}_7\text{M}_2\text{Mg}_7(\text{PO}_4)_{12}$ ($Z = 4$), where the $M = \text{Ca}, \text{Mg}, \text{Fe}^{2+}$. Stanfieldite from Brahin and a majority of other meteorites correspond to a composition with an intermediate $\text{Ca} \approx \text{Mg}$ occupancy of the $M5A$ site, leading to the overall formula $\sim \text{Ca}_7(\text{CaMg})\text{Mg}_9(\text{PO}_4)_{12} \equiv \text{Ca}_4\text{Mg}_5(\text{PO}_4)_6$. The mineral from the Lunar sample “rusty rock” 66095 approaches the $M = \text{Mg}$ end member, $\text{Ca}_7\text{Mg}_2\text{Mg}_9(\text{PO}_4)_{12}$. In lieu of any supporting analytical data, there is no evidence that the phosphor base with the formula $\text{Ca}_3\text{Mg}_3(\text{PO}_4)_4$ does exist.

Keywords: stanfieldite; phosphate; crystal structure; merrillite; meteorite; pallasite; mesosiderite; luminophore; bioceramics; powder diffraction; Raman spectroscopy

1. Introduction

It is known that the speciation of chemical elements in meteoritic substance significantly differs from their speciation in contemporary terrestrial lithosphere [1]. Concerning phosphorus, the main geochemical factors governing the diversity of terrestrial phosphorus-bearing minerals are (1) highly oxidative conditions typical of the present Earth and (2) the aquatic environment, which dramatically multiplies the number of possible pathways for phosphate geosynthesis. Contrary to Earth, the reductive and (in general) water-free conditions that accompanied the formation and early evolution of celestial bodies determined the limited number of meteoritic phosphorus-bearing minerals [2].

The most common meteoritic phosphates are the minerals related to the join merrillite–ferromerrillite, $\text{Ca}_9\text{NaMg}(\text{PO}_4)_7$ – $\text{Ca}_9\text{NaFe}^{2+}(\text{PO}_4)_7$ [3,4]. They are the typical accessories of ordinary chondrites, lunar rocks, martian meteorites, iron and stony-iron meteorites [3–6]. Chlorapatite, $\text{Ca}_5(\text{PO}_4)_3\text{Cl}$, is the second abundant phosphate in meteorites [2]. A series of Mg-rich phosphates are characteristic of stony-iron meteorites—pallasites and mesosiderites [6,7]. These minerals usually occur in association with schreibersite, $(\text{Fe,Ni})_3\text{P}$, and because of that, they are used for the assessment of phosphide–phosphate redox equilibria [8]. Stanfieldite, $\sim\text{Ca}_4\text{Mg}_5(\text{PO}_4)_6$, is the most common phosphate in the given assemblages [6,7]. The mineral was discovered in the Estherville mesosiderite [9] and is recognized in all well-studied pallasites [6,7,9–13], several mesosiderites [14,15] and even in the Lunar samples [16]. Being one of a very few Ca-rich phases occurring in pallasites, stanfieldite acts as a carrier of rare-earth elements substituting for Ca, and thereby is used in the studies of REE distribution among these meteorites [10,17]. Based on the overall observations and experimental data, stanfieldite can be regarded a late-stage cumulate of silicate-phosphate melts [18]. It is noteworthy that, in spite of an ordinary, “rock-forming” set of elements in the chemical composition, stanfieldite has never been encountered in terrestrial rocks. However, the phosphate identifiable as stanfieldite was reported as a constituent of prehistoric slags in Tyrol, Austria [19], and phosphorus-doped basaltic melts [20]. Stanfieldite of technogenic origin was detected as a component of bone-repairing bioceramics [21–28] and incinerated phosphate-based fertilizers [29–32].

In view of the notable role of stanfieldite in the mineralogy of pallasites, it looks unusual that the data on its chemical composition are rather ambiguous. The formula was first reported as $\text{Ca}_4\text{Mg}_5(\text{PO}_4)_6$ [9], but later on, the variations in the Ca/Mg ratio were shown to exist [12], and in many cases, stanfieldite formula is oversimplified as $\text{Ca}_3\text{Mg}_3(\text{PO}_4)_4$, e.g., Reference [33]. Synthetic $\text{Ca}_3\text{Mg}_3(\text{PO}_4)_4$ was reported as a phase in the $\text{Ca}_3(\text{PO}_4)_2$ – $\text{Mg}_3(\text{PO}_4)_2$ system [34], and nowadays, the compounds having the same inferred formula are widely explored as luminophores (e.g., References [35–39]). However, the powder XRD (X-ray diffraction) data given in these works [35–39] refer not to $\text{Ca}_3\text{Mg}_3(\text{PO}_4)_4$ but to the compound $\text{Ca}_7\text{Mg}_9(\text{Ca,Mg})_2(\text{PO}_4)_{12}$ [40], which was erroneously mislabeled as “ $\text{Ca}_3\text{Mg}_3(\text{PO}_4)_4$ ” both in ICSD and ICDD databases. Synthetic $\text{Ca}_7\text{Mg}_9(\text{Ca,Mg})_2(\text{PO}_4)_{12}$ was shown to have the same cell metrics as natural stanfieldite but it crystallizes in a different space group [9,40]. The latter discrepancy was discussed by Steele and Olsen in the abstract devoted to a crystal structure of natural stanfieldite [41]. However, no further structural data were provided by these authors, and as a consequence, no crystal structure of natural stanfieldite is available so far. In the course of a research of phosphate–phosphide assemblages of iron and stony-iron meteorites, we have found well-crystallized stanfieldite in the Brahin meteorite and carried out the detailed study of this mineral. We herein present the results and try to resolve some ambiguities related to a crystal chemistry of natural stanfieldite and its synthetic analogues.

2. Stanfieldite in the Brahin Pallasite

Brahin is a meteorite related to the main-group pallasites. It was first found in 1810 as two fragments (masses) of total weight ~ 80 kg at the Kaporenki village, Brahin district, Belarus. Since then, a few larger masses were recovered in the same district in 1968 and 2002. Nowadays, the total known weight of Brahin exceeds 800 kg [42]. Like other main-group pallasites, Brahin consists of round, nut-like and fragmented olivine crystals embedded into the Fe–Ni metal matrix. The less-common minerals are represented by schreibersite–nickelphosphide (Fe_3P – Ni_3P), chromite, troilite and daubreelite, FeCr_2O_4 . The specific feature of oxygen-bearing minerals of Brahin is their depletion in Mn [12]. Phosphates are comprised by merrillite, $\text{Ca}_9\text{NaMg}(\text{PO}_4)_7$, and stanfieldite. The crystal structure of iron-free merrillite from this meteorite has been recently reported [4]. Stanfieldite in Brahin was studied with respect to the occurrence of fission tracks [43]. A 1×2 mm grain of colorless stanfieldite was found in the centimeter-sized Brahin fragment kindly provided for the study by the Mining Museum, Saint Petersburg Mining University (specimen M65/2, which originates from the first find in 1810).

Stanfieldite and merrillite fill up the pocket bound by the fragmented olivine grains, schreibersite and (Fe, Ni) metal (Figure 1).

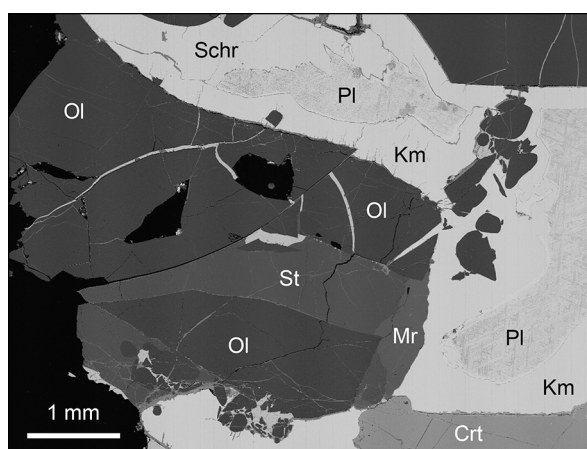


Figure 1. Stanfieldite (St) in the Brahin pallasite. Associated minerals: Ol, olivine; Mr, merrillite; Crt, chromite; Schr, schreibersite; Km, kamacite, α -(Fe,Ni); Pl, plessite (fine-grained aggregate of α - and γ -(Fe, Ni)). Polished section. SEM image of backscattered electrons. Image made by S.N.B.

3. Materials and Methods

A piece of the Brahin pallasite was polished and coated with a carbon film for electron microprobe study. SEM imaging (Figure 1) and microprobe analysis for the main elements were conducted by means of a CamScan 4 scanning electron microscope (SEM) (Cambridge, UK) equipped with a LINK AN1000 energy-dispersive analyzer (LINK Analytical, CA, USA). The following standards were used: chlorapatite (Ca-K, P-K), enstatite (Mg-K), hematite (Fe-K). The analysis was carried out at 20 kV acceleration voltage, 0.8 nA beam current, 1 μ m estimated beam diameter and 60 s live acquisition time per spot. The check-up for minor constituents was performed with a Microspec WDX-2 wavelength-dispersive X-ray spectrometer (Microspec Corporation, CA, USA) attached to the same SEM. The Mn content was determined using Mn- $K\alpha$ line (MnCO₃ standard) at 20 kV and 15 nA, whereas the contents of Ni, Co, Na, K and Si were found to lie below the detection limit (less than 0.05 wt.%).

For the purposes of the X-ray structural study, the grain of stanfieldite was extracted from the section and crushed into a few fragments, which were examined under a polarizing microscope in the immersion oil. Several optically homogeneous grains were checked using a Rigaku Oxford diffraction Xcalibur single-crystal diffractometer equipped with a fine-focus sealed tube and graphite monochromator (MoK α , 50 kV, 40 mA). It was found that all checked fragments are optically irresolvable intergrowths, each of them being composed of two or more domains misoriented within 5–10°. The best selected two-domain grain (0.15 \times 0.10 \times 0.10 mm) was glued onto a plastic loop and subjected to further data collection. A hemisphere of reciprocal space was collected up to 70° at room temperature, and the details are provided in Table 1. Subsequent data processing routines (integration, scaling and SHELX files setup) were performed by means of a CrysAlisPro software (Rigaku Oxford diffraction) [44]. The crystal structure has been solved using an intrinsic phasing approach and refined by means of a SHELX-2018 set of programs [45] incorporated into the Olex2 operation environment [46]. The details of structure refinement are given in Table 1 and in the crystallographic information file (CIF) attached to the Supplementary Materials (S1).

Table 1. Crystal data, single-crystal and Rietveld refinement details for stanfieldite from Brahin.

Crystal Data:	Single Crystal	Rietveld Method
Crystal system, space group	Monoclinic, <i>C2/c</i>	Monoclinic, <i>C2/c</i>
Crystal size (mm)	0.15 × 0.10 × 0.10	ball Ø 0.15
<i>a</i> (Å)	22.7973(4)	22.8036(2)
<i>b</i> (Å)	9.9833(2)	9.9832(1)
<i>c</i> (Å)	17.0522(3)	17.0558(2)
β (°)	99.954(2)	99.964(1)
<i>V</i> (Å ³)	3822.5(1)	3824.2(1)
<i>Z</i>	4	4
<i>D_x</i> (g cm ⁻³)	2.990	2.988
Data collection and refinement: Single Crystal		
Diffractometer	Rigaku Oxford Diffraction Xcalibur EoS	
Radiation	MoK α	
μ (mm ⁻¹)	2.12	
No. of meas., independent and obs. [<i>I</i> > 2 σ (<i>I</i>)] reflections	18,163, 5420, 3949	
<i>h, k, l</i> range	-27→32; -14→13; -23→23	
<i>R</i> _{int} , <i>R</i> _{σ}	0.044, 0.048	
<i>R</i> ₁ ($ F_o \geq 4\sigma_F$), <i>wR</i> ₂ , <i>GoF</i>	0.034, 0.082, 0.92	
$\Delta\sigma_{\min}$, $\Delta\sigma_{\max}$ (e Å ⁻³)	-0.56, 0.86	
Data collection and refinement: Rietveld method		
Diffractometer	Rigaku RAXIS Rapid II (imaging plate)	
Radiation	CoK α_1 /CoK α_2	
μ (mm ⁻¹)	26.11	
Exposure time (s)	1800	
Calculation step (°)	0.02	
2 Θ range (°)	6–132	
Peak shape description	Modified Pseudo-Voigt	
Background subtraction	28-coefficient Chebyshev polynomial	
<i>R_p</i> , <i>R_{wp}</i> , <i>R_B</i> (%), <i>GOF</i>	0.39, 0.69, 0.41, 1.79	

The X-ray powder diffraction pattern (Table 2) was obtained with a Rigaku R-AXIS Rapid II diffractometer (Rigaku Corporation, Tokyo, Japan) equipped with a curved (semi-cylindrical) imaging plate. A ~150 μm ball was prepared from the stanfieldite powder mixed with an epoxy resin and was picked onto a glass fiber. The image acquisition conditions were: CoK α -radiation, rotating anode with microfocus optics, 40 kV, 15 mA, Debye-Scherrer geometry, $r = 127.4$ mm, exposure 30 min. The imaging plate was calibrated against Si standard. The image-to-profile data conversion was performed with an osc2xrd program [47]. The unit-cell parameters and occupancies of Mg1–Mg5 sites were refined by the Rietveld method (Table 1, Figure 2) using Bruker TOPAS v. 5.0 software (Bruker Inc., Wisconsin). The occupancies at the M5A site were fixed at the values determined by single-crystal refinement. The atomic coordinates were not refined but were fixed according to single-crystal data. The XPRD pattern (Table 2) was indexed on the basis of theoretical values calculated with STOE WinXPOW v. 1.28 software (Stoe & Cie GmbH, Darmstadt, Germany).

The micro-Raman spectrum was recorded from a random powder sample using a Horiba Jobin-Yvon LabRam 800 instrument (HORIBA Jobin Yvon GmbH, Bensheim, Germany), equipped with a 50 \times confocal objective. The instrument was operated with a 514 nm Ar⁺ laser at a 1 nm lateral resolution and 2 cm⁻¹ spectral resolution. The optics were preliminarily calibrated using a Si reflection standard.

Table 2. X-ray powder diffraction data (d in Å) for stanfieldite from the Brahin meteorite.

I_{meas}	d_{meas}	I_{calc}^1	d_{calc}	hkl	I_{meas}	d_{meas}	I_{calc}^1	d_{calc}	hkl
1	11.31	2	11.23	200	48	2.500	30	2.500	623
1	9.13	<1	9.12	110			20	2.496	040
23	8.32	21	8.26	-111	4	2.423	4	2.420	910
<1	6.26	1	6.23	202	6	2.401	6	2.398	241
23	6.00	21	5.97	112	2	2.379	2	2.377	-823
<1	5.625	<1	5.614	400	4	2.343	3	2.341	911
3	5.424	2	5.409	311	3	2.319	1, 1	2.322	135, 533
3	5.247	2	5.230	-312	5	2.295	5	2.293	624
4	5.108	3	5.091	-402	6	2.283	1, 3	2.281	-441, 440
16	5.006	13	4.992	020	8	2.259	6	2.257	-716
2	4.800	1	4.785	021	2	2.240	1, 1	2.240	-442, 441
1	4.662	1	4.629	113	5	2.205	3	2.202	-626
4	4.604	3	4.585	312	9	2.161	3	2.163	027
2	4.406	0.5	4.405	-313			2	2.160	-136
3	4.334	2	4.326	221			2	2.159	732
5	4.186	4	4.177	-204	4	2.138	1, 1	2.138	-734, -825
3	4.104	2	4.096	510	9	2.127	5, 4	2.126	823, 426
42	3.849	36	3.842	511	3	2.077	2	2.076	640
			3.742	600	2	2.066	1, 1	2.066	-10.2.2, 227
			3.733	-421	2	2.028	1	2.029	-10.2.3
100	3.738	100	3.730	420	7	2.006	2	2.008	-245
			3.727	204			2	2.003	045
			3.726	023			2	2.001	-518
10	3.688	8	3.681	-404	4	1.960	5	1.960	914
3	3.592	3	3.586	-513	2	1.901	1, 1	1.901	-736, 318
2	3.282	2	3.272	422	3	1.884	2	1.883	-153
9	3.248	7	3.246	-131	15	1.867	4	1.871	12.0.0
		2	3.234	314			8	1.867	-842
3	3.217	1	3.213	024			4	1.864	408
2	3.118	1	3.114	404			4	1.863	046
10	3.087	7.2	3.083	115, 513	7	1.840	7	1.841	-808
18	3.042	15	3.039	132	3	1.827	1, 1	1.828	841, 915
7	2.955	6	2.952	423	4	1.801	4	1.800	551
2	2.873	2	2.870	-133	2	1.789	2	1.787	-338
10	2.834	7	2.834	-206	3	1.753	1, 2	1.751	-429, 138
		12	2.825	-515	2	1.742	1, 1	1.742	-247, -538
83	2.807	26	2.812	-802	3	1.697	2	1.697	11.1.4
		27	2.807	800	2	1.652	2	1.653	-555
		24	2.800	-225	3	1.621	2, 2	1.622	-356, 10.0.6
12	2.731	3.5	2.730	-116, 712	3	1.605	2	1.605	-829
6	2.706	5	2.705	622	6	1.597	6	1.597	429
13	2.685	11	2.682	-316	3	1.543	3	1.543	339
2	2.639	2	2.642	424	3	1.516	2	1.515	-13.1.7
2	2.621	2	2.627	-532	3	1.481	2	1.481	-848
3	2.601	4	2.599	531					

¹ Intensities were normalized to $\Sigma I[(600) + (-421) + (420) + (204) + (023)] = 100$. Reflections having relative intensity less than 2 at $d < 4.00$ Å have been omitted.

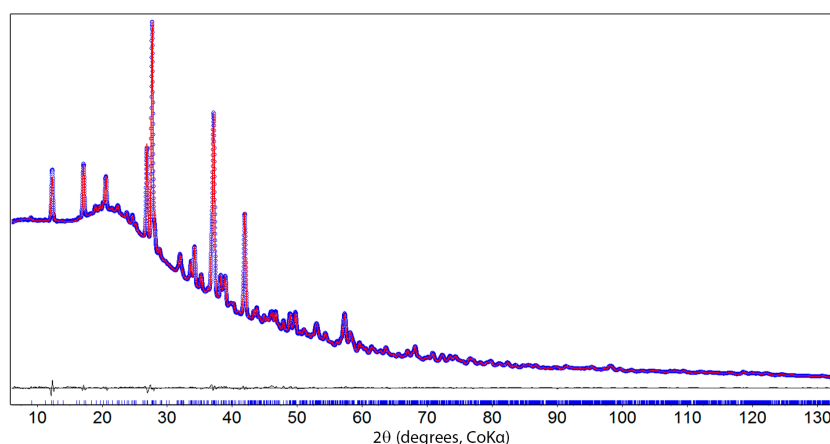


Figure 2. Rietveld refinement plot of stanfieldite from the Brahin meteorite.

4. Results and Discussion

4.1. Stanfieldite: A Complete Structure-Composition Dataset

The X-ray examination of Brahin stanfieldite was carried out by two different methods. Both single-crystal and Rietveld refinements of the unit cell had led to almost identical parameters (deviation between the unit-cell volumes is 0.04%, Table 1). The refined Mg/Fe occupancies were also well converged (Table 3). The chemical composition of studied stanfieldite (wt.%, average of 3 points): CaO 26.21, MgO 21.66, FeO 3.02, MnO 0.27, P₂O₅ 49.38, total 100.54 can be recalculated to the formula Ca_{8.04}Mg_{9.25}Fe_{0.72}Mn_{0.07}P_{11.97}O₄₈. The latter is close to the composition determined by the structure refinement, Ca_{7.97}Mg_{9.47}Fe_{0.56}P₁₂O₄₈. Based on these results, one can state that the bond lengths and derivative bond-valence sums (Table 3) are herein calculated with a good confidence.

Fuchs [9], in 1969, could reliably determine the unit-cell metrics, but misrecognized the space group of the mineral (Table 4), perhaps due to the same pseudo-twinning of the crystals [40,41] which we observed on our studied stanfieldite.

Table 3. Selected structural parameters of cation sites in natural and synthetic stanfieldite ¹.

Site	CN ²	Length ³	BVS ⁴	Mg ⁵	Length ³	BVS ⁴	Length ³	Mg ⁵
Brahin (Present Work)				Ca ₇ (Ca,Mg)Mg ₉ (PO ₄) ₁₂ Synthetic [40]		Imilac [41]		
Ca1 (4e)	8	2.543	1.86		2.547	1.85	2.542	
Ca2 (8f)	7	2.445	2.09		2.444	2.10	2.445	
Ca3 (8f)	8	2.566	1.69		2.569	1.68	2.573	
Ca4 (8f)	8	2.496	2.02		2.498	2.01	2.498	
Mg1 (4e)	4	1.995	1.79	0.934(5)/0.91	1.999	1.75		0.928(4)
Mg2 (8f)	6	2.096	2.08	0.945(3)/0.94	2.095	2.07	2.097	0.942(3)
Mg3 (8f)	5	2.068	1.83	0.985(4)/0.98	2.071	1.81		0.969(3)
Mg4 (8f)	5	2.049	1.92	0.983(3)/1.00	2.054	1.89		0.980(3)
Mg5 (8f)	6	2.132	1.89	0.919(3)/0.90	2.130	1.88		0.903(3)
M5A (8f)	6	2.257	1.89	See Table 5	2.270	1.92	2.282	
P1 (8f)	4	1.535	4.83		1.540	4.76		
P2 (8f)	4	1.535	4.83		1.538	4.79		
P3 (8f)	4	1.537	4.81		1.541	4.75		
P4 (8f)	4	1.532	4.85		1.538	4.78		
P5 (8f)	4	1.534	4.83		1.536	4.81		
P6 (8f)	4	1.530	4.89		1.532	4.86		

¹ Complete listings of atomic coordinates, thermal displacement parameters and bond lengths are given in Supplementary Tables S1–S3. ² CN, coordination number. ³ Average cation-oxygen bond lengths (Å). ⁴ BVS, bond-valence sums (in valence units), calculated by summation of individual element contributions based on parameters reported by Brese and O’Keeffe [48]. ⁵ Refined Mg occupancies for Mg1–Mg5 sites. Data for Brahin include both single-crystal and Rietveld refinement results separated by slash.

Table 4. Unit cell parameters of natural and synthetic stanfieldite refined from single-crystal data.

Source	Brahin	Synthetic	Imilac	Estherville
Space group	C2/c	C2/c	C2/c	P2/c or Pc ¹
<i>a</i> (Å)	22.7973(4)	22.841(3)	22.81	17.16(3)
<i>b</i> (Å)	9.9833(2)	9.994(1)	9.993	10.00(2)
<i>c</i> (Å)	17.0522(3)	17.088(5)	17.09	22.88(4)
β (°)	99.954(2)	99.63(3)	99.96	100.3(2)
<i>V</i> (Å ³)	3822.5	3845.8	3836.8	3862.9
Reference	This work	[40]	[41]	[9]

¹ Space group assignment and cell axes permutation are discussed in References [40,41].

Dickens and Brown [40] have synthesized the synthetic, Fe-free analogue of stanfieldite and thoroughly described its crystal structure. However, the latter authors did not perform independent determination of the chemical composition of synthesized material—as one will see, this is an essential requirement in view of the widely varying composition of at least one structural site of stanfieldite. Steele and Olsen [41] have reported the preliminary results of structural examination of natural stanfieldite from the Imilac pallasite. They gave the analytical chemical formula of the mineral, but did not provide full structural data, confining the results to unit cell metrics, average bond lengths and selected site occupancies (Tables 3 and 4). As a consequence, no complete structure-composition dataset for stanfieldite is available so far, and the data provided herein are the first report of that type.

4.2. General Features of Stanfieldite Structure and Its Formula

The crystal structure of stanfieldite is a complex framework composed of 10 metal sites and 6 phosphate groups (Table 3, Figure 3, Supplementary Table S1). Dickens and Brown [40] gave the detailed description of each site in the structure of synthetic analogue of the mineral, and the present paragraph aims to overview stanfieldite structure and highlight its features. The most interesting one is a pseudo-hexagonal character of the framework which can be best viewed via the arrangement of [PO₄] tetrahedra along the [10–2] axis (Figure 3A). In principle, stanfieldite, being presented by the oversimplified formula $M_3(\text{PO}_4)_2$ ($M = \text{Mg, Ca}$; $Z = 24$), can be regarded as a derivative of the well-known glaserite structure type, $\text{K}_3\text{Na}(\text{SO}_4)_2$ [49,50]. Dickens and Brown [40] discuss the relationships between stanfieldite and glaserite-related phosphates belonging to α - and β - $\text{Ca}_3(\text{PO}_4)_2$ structural types. The latter is known as a basement of whitlockite-group mineral structures [51], two of which, merrillite and ferromerrillite, are of fundamental importance in the mineralogy of meteorites [3,4]. In view of the common and intimate association of stanfieldite and merrillite in pallasite meteorites (Figure 1), these relationships could be of particular interest. However, contrary to Dickens and Brown [40], we would not overestimate the similarity of stanfieldite and merrillite structures. The unusual face-sharing of adjacent [MO₆] octahedron and [PO₄] tetrahedron characteristic of merrillite [3] does not occur in stanfieldite structure.

The refinement of occupancies of four Ca-sites in the stanfieldite structure showed no evidence for either Mg or Fe substitution. However, refinement of four Mg sites using both single-crystal and Rietveld methods concordantly leads to a partial substitution of Mg for Fe, with iron being preferentially concentrated in Mg1 (tetrahedral) and Mg5 (octahedral) positions (Table 3). The tetrahedral coordination of Mg1 is highly unusual; however, it is sometimes encountered in mineral structures such as åkermanite, $\text{Ca}_2\text{MgSi}_2\text{O}_7$ (melilite structure type), and spinel. The M5A site allows mixed occupancy by Ca, Mg and Fe, and thus will be discussed in the next section. Based on the structural data, the overall formula of stanfieldite can be written as $\text{Ca}_7\text{M}_2\text{Mg}_9(\text{PO}_4)_7$, where $M = \text{Ca, Mg or Fe}^{2+}$.

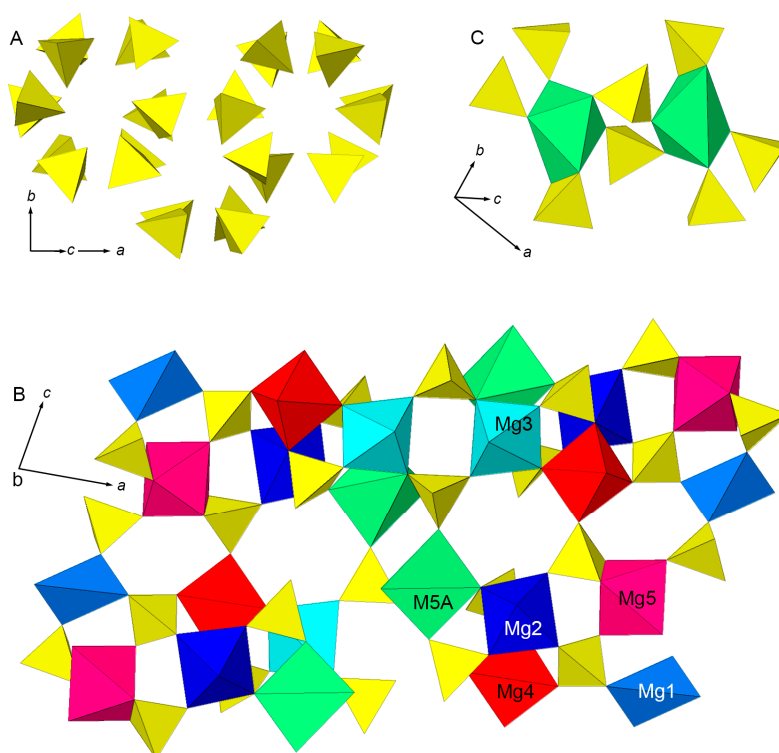


Figure 3. Crystal structure of stanfieldite. (A) Pseudo-hexagonal stacking of [PO₄] tetrahedra (yellow), projection along the [10-2] axis. The cations were hidden for clarity. (B) A slice of the structure on {010}. Arrangement of Mg-polyhedra and [PO₄] tetrahedra. Ca atoms reside in the spaces and have been hidden for clarity. (C) A view of a pair of distorted [M5AO₆] octahedra corner-linked by [PO₄] tetrahedra.

4.3. The M5A Site, A Key to A Flexibility of Stanfieldite Composition

This cation site (which was previously referred to as Ca5 [40]) deserves a special discussion as it determines the variability of stanfieldite composition which, in turn, has led to misinterpretations of the chemical formula of the mineral and its synthetic analogues. The central atom resides in the general 8f position and coordinates to six oxygen atoms to form a highly distorted octahedron (Figure 3C), with the bond distances varying from 2.1 to almost 2.5 Å (Table 5).

Table 5. Bond lengths (Å), bond-valence sums (BVS, valence units) and occupancy factors for the M5A site of stanfieldite and its synthetic analogue ¹.

	Brahin	Synthetic	Imilac
M5A—O4	2.194(2)	2.212(3)	
M5A—O5	2.291(2)	2.302(3)	
M5A—O18	2.494(2)	2.493(3)	
M5A—O19	2.200(2)	2.223(4)	
M5A—O22	2.099(3)	2.107(4)	
M5A—O23	2.262(3)	2.282(4)	
Mean M5A—O	2.257	2.270	2.282
BVS	1.89	1.92	
Ca	0.48(4)	0.51	0.55
Mg	0.43(2)	0.49	0.353(3)
Fe ²⁺	0.08(2)		0.097(3)
Reference	This work	[40]	[41]

¹ Bond-valence sums were calculated by summation of individual contributions for each element, based on parameters reported by Brese and O’Keeffe [48].

The M5A octahedra form paired clusters in the structure via corner-linking by phosphate tetrahedra (Figure 3C). Based on previous reports [40,41,52] and our data (Table 5), M5A may accommodate Ca, Mg, Fe²⁺ and Ni in different proportions, with the total occupancy equal to unity. Natural stanfieldite is a Mg-dominant mineral, and the refinement of M5A occupancy leads to a dominance of Mg over Fe²⁺ as well (Table 5). The latter is supported by calculation of the bond-valence sum, which is almost identical to that of synthetic analogue of stanfieldite (Table 3). The variability of M5A occupancy substantiates the existence of solid solution between hypothetical Mg and Ca end members.

The former would have the composition corresponding to Ca₇Mg₂Mg₉(PO₄)₁₂. The latter member would correspond to Ca₇Ca₂Mg₉(PO₄)₁₂, that is equal to Ca₃Mg₃(PO₄)₄. The intermediate composition having Ca = Mg in M5A results in a formula Ca₇(CaMg)Mg₉(PO₄)₁₂, or, in a simplified form, Ca₄Mg₅(PO₄)₄. One can see that the latter perfectly fulfils the ideal composition of stanfieldite proposed by Fuchs [9]. It is noteworthy that stanfieldite from Brahin described herein, the previously reported mineral from Imilac [41] and the synthetic analogue of stanfieldite [40] have M5A occupancies almost equally shared between Ca and (Mg + Fe) (Table 5). This could lead to the assumption that the ordering between Ca and Σ(Mg, Fe) might exist in the M5A site. However, neither our observations nor previously reported data reveal superstructure reflections which would evidence the Ca/Mg ordering. In this respect, an overview of reported compositions of stanfieldite-like minerals and compounds would be of special interest. We have collected the chemically relevant data which are gathered in Table 6 and plotted in Figure 4. It can be seen that the overwhelming majority of stanfieldite compositions fall within the range corresponding to Ca ≈ (Mg + Fe) in the M5A site. Therefore, the above assumption on the possible Ca/Mg ordering, albeit speculative, has a statistically substantiated basis.

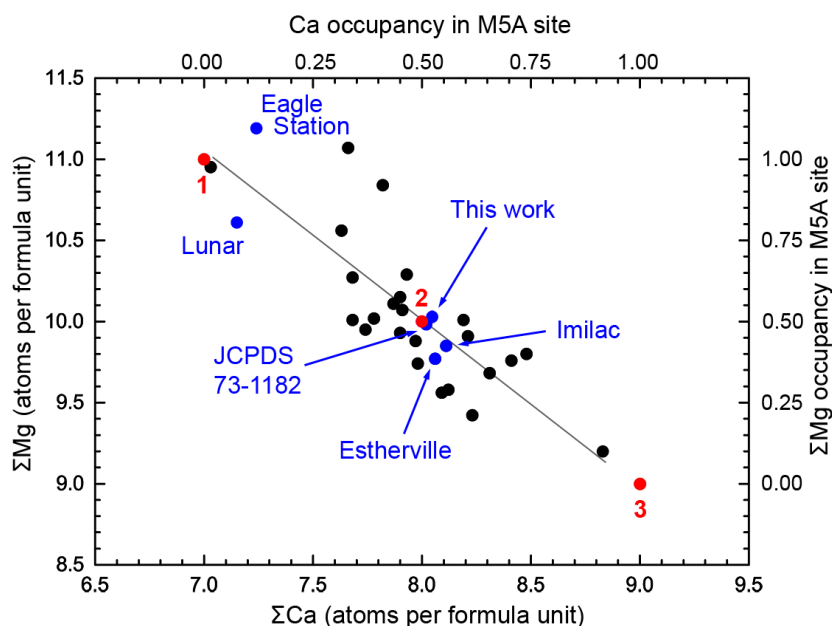


Figure 4. Plot of ΣCa versus ΣMg group element contents in natural, technogenic and synthetic stanfieldite. Left and bottom scale: formula amounts recalculated on the basis of 48 oxygen atoms per formula unit. Right and upper scale: expected occupancy factors for the M5A site. The grey straight line shows the linear fit for the depicted analytical data. The red dots denote theoretical (calculated) compositions corresponding to (1) Ca₇Mg₂Mg₉(PO₄)₁₂, (2) Ca₇(CaMg)Mg₉(PO₄)₁₂ \equiv Ca₄Mg₅(PO₄)₆, (3) Ca₇Ca₂Mg₉(PO₄)₁₂ \equiv Ca₃Mg₃(PO₄)₄. The blue dots and labels mark the compositions of particular interest which are discussed in the paper. References and source data are given in Table 6.

Table 6. Formula amounts of cations in stanfieldite and its analogues grouped by elements ¹.

Source ²	ΣCa ³	ΣMg ⁴	P + Si	Reference
Albin	8.23	9.42	12.15	[7]
Antofagasta	8.48	9.80	11.89	[7]
Antofagasta	8.41	9.76	11.93	[7]
Brahin	7.68	10.01	12.12	[43]
Brahin ⁵	8.04	10.03	11.97	
Eagle Station	7.63	10.56	11.93	[7]
Eagle Station	7.24	11.19	11.86	[7]
Eagle Station	7.78	10.02	12.08	[10]
Estherville	8.06	9.77	12.07	[9]
Imilac	7.91	10.07	12.04	[7]
Imilac	8.11	9.85	12.02	[41]
<i>Lunar</i>	7.15	10.61	12.12	[16]
Mt. Vernon	8.21	9.91	11.95	[7]
Mt. Vernon	8.09	9.56	12.14	[7]
Mt. Vernon	8.31	9.68	12.02	[7]
Ollague	8.19	10.01	11.92	[7]
Rawlinna	7.66	11.07	11.79	[7]
Rawlinna	7.82	10.84	11.73	[7]
Santa Rosalia	7.90	9.93	12.08	[7]
Santa Rosalia	8.12	9.58	12.13	[7]
Santa Rosalia	7.98	9.74	12.11	[7]
Springwater	7.97	9.88	12.08	[7]
Springwater	7.74	9.95	12.14	[7]
Springwater	7.90	10.15	12.00	[7]
Springwater	7.87	10.11	12.01	[10]
Vaca Muerta	7.93	10.29	11.97	[15]
<i>Slags</i>	8.83	9.20	12.01	[19]
<i>Slags</i>	7.03	10.95	12.04	[19]
<i>Slags</i>	7.68	10.27	12.05	[19]
<i>Synthetic</i>	8.02	9.98	12.00	[40]

¹ Atoms per formula unit calculated on the basis of 48 oxygen atoms. ² Meteorite names. Non-meteoritic sources are shown in italic type. ³ ΣCa includes (Ca, Na, K). ⁴ ΣMg includes (Mg, Fe, Mn, Al, Cr, Ti). ⁵ Present work.

The next interesting point is a significant departure of total cationic sums of many analyses from the ideal value requiring 18 cations per formula unit. These departures are readily revealed by the shifts of corresponding analytical points from the linear fit in Figure 4. At present, we have no explanation for the observed departures. They could imply the existence of analytical errors in the reported microprobe data. On the other hand, these shifts might mean the occurrence of vacancies in cationic sites of stanfieldite structure, and then they deserve a special investigation.

Although the majority of reported data fall within the central area of the plot in Figure 4, there are a few points showing significant prevalence of (Mg + Fe) sum over total Ca. These include one analysis from the Eagle Station pallasite [7] and the mineral found in the Lunar sample 66095 returned by the Apollo 16 mission [16]. These two analyses approach the $\text{Ca}_7\text{Mg}_2\text{Mg}_9(\text{PO}_4)_{12}$ end-member of the M5A solid solution. At the opposite extreme of the plot, there is a single point approaching hypothetical $\text{Ca}_3\text{M}_3(\text{PO}_4)_4$ composition. This analysis, along with two more listed in Table 6, relate to a stanfieldite-like phosphate described from the ancient slags found in Tyrol [19]. The main feature of this compound is wide variations both in Ca/(Fe + Mg) and Fe/Mg ratios, up to nearly Fe-dominant compositions. Schneider, with co-authors [19], has provided Raman spectrum for this phosphate, but in the absence of Raman spectra for genuine stanfieldite, the comparison was not possible. We herein provide the Raman spectrum of stanfieldite from the Brahın meteorite (Figure 5). A comparison of this spectrum with that reported by Schneider with co-authors [19] shows that the latter can represent a poorly crystallized Fe-dominant analogue of stanfieldite.

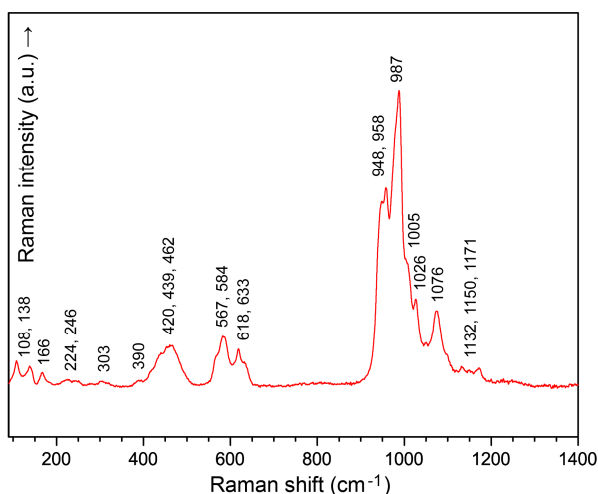


Figure 5. The Raman spectrum of stanfieldite from the Brahin meteorite. The bands between 900 and 1150 cm^{-1} correspond to stretching vibrations in $[\text{PO}_4]$ tetrahedra. Bands in the range 400–650 cm^{-1} relate to bending modes of phosphate anion.

5. $\text{Ca}_3\text{Mg}_3(\text{PO}_4)_4$ Phosphors: Do They Exist?

In this section, we would like to clarify the mistake caused by the incorrect database assertion of primary structural data on the synthetic analogue of stanfieldite reported by Dickens and Brown [40]. In the title of their article, Dickens and Brown report the formula $\text{Ca}_7\text{Mg}_9(\text{Ca},\text{Mg})_2(\text{PO}_4)_{12}$, with $\text{Ca} = \text{Mg}$ in the Ca5 site, leading to a bulk one $\text{Ca}_4\text{Mg}_5(\text{PO}_4)_6$. It looks obvious that the mistake was introduced in the stage of structural data transfer from the article tables to the ICSD database. The Ca5 site, equally occupied by Ca and Mg [40], was erroneously assigned to be fully occupied by Ca. The latter had led to a wrong formula, $\text{Ca}_3\text{Mg}_3(\text{PO}_4)_4$, which still appears in the ICSD database [53] (ICSD code 23642). Moreover, the calculated X-ray powder diffraction pattern has been further included into the ICDD (JCPDS) database under the reference number JCPDS-ICDD 73-1182 (Figure 4). There is a substantial interest to the family of luminophores (phosphors) based on the stanfieldite structure [35–39]. It is erroneous that the mistake in the chemical formula caused by the incorrect primary data transfer has passed first to the ICDD database and then to the papers devoted to a study of these phosphor materials [35–39]. Unfortunately, neither of the published articles does contain quantitative chemical data on synthesized phosphors. Thus, in lieu of any evidence supporting the existence of $\text{Ca}_3\text{Mg}_3(\text{PO}_4)_4$, one can state that these phosphors are in fact stanfieldite-based, $\text{Ca}_4\text{Mg}_5(\text{PO}_4)_4$ compounds.

Supplementary Materials: The following are available online at <http://www.mdpi.com/2073-4352/10/6/464/s1>: Supplementary crystallographic data for stanfieldite from the Brahin meteorite in Crystallographic Information File (CIF) format. Alternatively, CCDC reference number 1998335 contains the same data, and it can be obtained free of charge from the Cambridge Crystallographic Data Centre at www.ccdc.cam.ac.uk. S2, supplementary crystallographic Tables S1–S3.

Author Contributions: Conceptualization, writing—original draft preparation, S.N.B.; investigation, S.N.B., M.G.K. and V.N.B.; data curation, E.V.O. All authors have read and agreed to the published version of the manuscript.

Funding: This research was financially supported by the Russian Science Foundation, grant number 18-17-00079.

Acknowledgments: The authors gratefully acknowledge the curators of the Mining Museum, Saint Petersburg Mining University, for providing the sample of the Brahin meteorite used in this study. We are thankful to anonymous reviewers for their comments and suggestions. This research was supported by the resource Centre for X-ray diffraction studies and the Geomodel resource centre of Saint Petersburg State University.

Conflicts of Interest: The authors declare no conflict of interest.

References

1. Hystad, G.; Downs, R.T.; Grew, E.S.; Hazen, R.M. Statistical analysis of mineral diversity and distribution: Earth's mineralogy is unique. *Earth Planet Sci. Lett.* **2015**, *426*, 154–157. [[CrossRef](#)]
2. Rubin, A.E.; Ma, C. Meteoritic minerals and their origins. *Chem. Erde—Geochem.* **2017**, *77*, 325–385. [[CrossRef](#)]
3. Jolliff, B.L.; Hughes, J.M.; Freeman, J.J.; Zeigler, R.A. Crystal chemistry of lunar merrillite and comparison to other meteoritic and planetary suites of whitlockite and merrillite. *Am. Mineral.* **2006**, *91*, 1583–1595. [[CrossRef](#)]
4. Britvin, S.N.; Krivovichev, S.V.; Armbruster, T. Ferromerrillite, $\text{Ca}_9\text{NaFe}^{2+}(\text{PO}_4)_7$, a new mineral from the Martian meteorites, and some insights into merrillite-tuite transformation in shergottites. *Eur. J. Mineral.* **2016**, *28*, 125–136. [[CrossRef](#)]
5. Lewis, J.A.; Jones, R.H. Phosphate and feldspar mineralogy of equilibrated L chondrites: The record of metasomatism during metamorphism in ordinary chondrite parent bodies. *Meteor. Planet. Sci.* **2016**, *51*, 1886–1913. [[CrossRef](#)]
6. Buseck, P.R. Pallasite meteorites—Mineralogy, petrology and geochemistry. *Geochim. Cosmochim. Acta* **1977**, *41*, 711–740. [[CrossRef](#)]
7. Buseck, P.B.; Holdsworth, E.F. Phosphate minerals in pallasite meteorites. *Mineral. Mag.* **1977**, *41*, 91–102. [[CrossRef](#)]
8. Righter, K.; Arculus, R.J.; Paslick, C.; Delano, J.W. Electrochemical measurements and thermodynamic calculations of redox equilibria in pallasite meteorites—Implications for the eucrite parent body. *Geochim. Cosmochim. Acta* **1990**, *54*, 1803–1815. [[CrossRef](#)]
9. Fuchs, L.H. Stanfieldite: A new phosphate mineral from stony-iron meteorites. *Science* **1967**, *158*, 910–911. [[CrossRef](#)]
10. Davis, A.M.; Olsen, E.J. Phosphates in pallasite meteorites as probes of mantle processes in small planetary bodies. *Nature* **1991**, *353*, 637–640. [[CrossRef](#)]
11. Sharygin, V.V.; Kovyazin, S.V.; Podgornykh, N.M. Mineralogy of olivine-hosted inclusions from the Omolon pallasite. In Proceedings of the 37th Annual Lunar and Planetary Science Conference, League City, TX, USA, 13–17 March 2006. abstract no. 1235.
12. Boesenberg, J.S.; Delaney, J.S.; Hewins, R.H. A petrological and chemical reexamination of Main Group pallasite formation. *Geochim. Cosmochim. Acta* **2012**, *89*, 134–158. [[CrossRef](#)]
13. McKibbin, S.J.; Pittarello, L.; Makarona, C.; Hamann, C.; Hecht, L.; Chernonozhkin, S.M.; Goderis, S.; Claeys, P. Petrogenesis of main group pallasite meteorites based on relationships among texture, mineralogy, and geochemistry. *Meteor. Planet. Sci.* **2019**, *54*, 2814–2844. [[CrossRef](#)]
14. Kong, P.; Su, W.; Li, X.; Spettel, B.; Palme, H.; Tao, K. Geochemistry and origin of metal, olivine clasts, and matrix in the Dong Ujimqin Qi mesosiderite. *Meteor. Planet. Sci.* **2008**, *43*, 451–460. [[CrossRef](#)]
15. Greenwood, R.C.; Barrat, J.-A.; Scott, E.R.D.; Haack, H.; Buchanan, P.C.; Franchi, I.A.; Yamaguchi, A.; Johnson, D.; Bevan, A.W.R.; Burbine, T.H. Geochemistry and oxygen isotope composition of main-group pallasites and olivine-rich clasts in mesosiderites: Implications for the “Great Dunite Shortage” and HED-mesosiderite connection. *Geochim. Cosmochim. Acta* **2015**, *169*, 115–136. [[CrossRef](#)]
16. Shearer, C.K.; Sharp, Z.D.; Burger, P.V.; McCubbin, F.M.; Provencio, P.P.; Brearley, A.J.; Steele, A. Chlorine distribution and its isotopic composition in “rusty rock” 66095. Implications for volatile element enrichments of “rusty rock” and lunar soils, origin of “rusty” alteration, and volatile element behavior on the Moon. *Geochim. Cosmochim. Acta* **2014**, *139*, 411–433. [[CrossRef](#)]
17. Hsu, W. Minor element zoning and trace element geochemistry of pallasites. *Meteor. Planet. Sci.* **2003**, *38*, 217–241. [[CrossRef](#)]
18. Tollari, N.; Toplis, M.J.; Barnes, S.-J. Predicting phosphate saturation in silicate magmas: An experimental study of the effects of melt composition and temperature. *Geochim. Cosmochim. Acta* **2006**, *70*, 1518–1536. [[CrossRef](#)]
19. Schneider, P.; Tropper, P.; Kaindl, R. The formation of phosphoran olivine and stanfieldite from the pyrometamorphic breakdown of apatite in slags from a prehistoric ritual immolation site (Goldbichl, Igls, Tyrol, Austria). *Mineral. Petrol.* **2013**, *107*, 327–340. [[CrossRef](#)]
20. Tarrago, M.; Garcia-Valles, M.; Martinez, S.; Pradell, T.; Bruna, P. Fe in P-doped basaltic melts: A Mössbauer spectroscopy study. *Mater. Lett.* **2018**, *228*, 57–60. [[CrossRef](#)]

21. LeGeros, R.Z.; Mijares, D.; Yao, F.; Tannous, S.; Catig, G.; Xi, Q.; Dias, R.; LeGeros, J.P. Synthetic bone mineral (SBM) for osteoporosis therapy: Part 1 - prevention of bone loss from mineral deficiency. *Key Eng. Mater.* **2008**, *361–363 Pt 1*, 43–46. [CrossRef]
22. Vorndran, E.; Ewald, A.; Müller, F.A.; Zorn, K.; Kufner, A.; Gbureck, U. Formation and properties of magnesium-ammonium-phosphate hexahydrate bioceramics in the Ca-Mg-PO₄ system. *J. Mater. Sci. Mater. Med.* **2011**, *22*, 429–436. [CrossRef] [PubMed]
23. Alkhraisat, M.H.; Cabrejos-Azama, J.; Rodriguez, C.R.; Jerez, L.B.; Cabarcos, E.L. Magnesium substitution in brushite cements. *Mater. Sci. Eng. C* **2013**, *33*, 475–481. [CrossRef] [PubMed]
24. Christel, T.; Geffers, M.; Klammert, U.; Nies, B.; Höß, A.; Groll, J.; Kübler, A.C.; Gbureck, U. Fabrication and cytocompatibility of spherical magnesium ammonium phosphate granules. *Mater. Sci. Eng. C* **2014**, *42*, 130–136. [CrossRef] [PubMed]
25. Khan, N.I.; Ijaz, K.; Zahid, M.; Khan, A.S.; Abdul Kadir, M.R.; Hussain, R.; Anis-ur-Rehman; Darr, J.A.; Ihtesham-ur-Rehman; Chaudhry, A.A. Microwave assisted synthesis and characterization of magnesium substituted calcium phosphate bioceramics. *Mater. Sci. Eng. C* **2015**, *56*, 286–293. [CrossRef]
26. Singh, S.S.; Roy, A.; Lee, B.; Banerjee, I.; Kumta, P.N. Synthesis, characterization, and in-vitro cytocompatibility of amorphous β -tri-calcium magnesium phosphate ceramics. *Mater. Sci. Eng. C* **2016**, *67*, 636–645. [CrossRef]
27. Blum, C.; Brückner, T.; Ewald, A.; Ignatius, A.; Gbureck, U. Mg:Ca ratio as regulating factor for osteoclastic in vitro resorption of struvite bioceramics. *Mater. Sci. Eng. C* **2017**, *73*, 111–119. [CrossRef]
28. Ammar, H.; Nasr, S.; Ageorges, H.; Salem, E.B. Sintering and mechanical properties of magnesium containing hydroxyfluorapatite. *J. Aust. Ceram. Soc.* **2019**, in press. [CrossRef]
29. Hernandez, A.B.; Ferrasse, J.-H.; Chaurand, P.; Saveyn, H.; Borschneck, D.; Roche, N. Mineralogy and leachability of gasified sewage sludge solid residues. *J. Hazard. Mater.* **2011**, *191*, 219–227. [CrossRef]
30. Zhang, Q.; Liu, H.; Li, W.; Xu, J.; Liang, Q. Behavior of phosphorus during co-gasification of sewage sludge and coal. *Energy Fuels* **2012**, *26*, 2830–2836. [CrossRef]
31. Qian, T.-T.; Jiang, H. Migration of phosphorus in sewage sludge during different thermal treatment processes. *ACS Sustain. Chem. Eng.* **2014**, *2*, 1411–1419. [CrossRef]
32. Zhao, Y.; Ren, Q.; Na, Y. Potential utilization of phosphorus in fly ash from industrial sewage sludge incineration with biomass. *Fuel Process. Technol.* **2019**, *188*, 16–21. [CrossRef]
33. Huminicki, D.M.C.; Hawthorne, F.C. The crystal chemistry of the phosphate minerals. In *Phosphates—Geochemical, Geobiological, and Materials Importance*; Reviews in Mineralogy and Geochemistry; Kohn, M.L., Rakovan, J., Hughes, J.M., Eds.; Mineralogical Society of America: Chantilly, VA, USA, 2002; Volume 48, p. 148.
34. Jumpei, A. Phase diagrams of Ca₃(PO₄)₂-Mg₃(PO₄)₂ and Ca₃(PO₄)₂-CaNaPO₄ systems. *Bull. Chem. Soc. Jpn.* **1958**, *31*, 201–205. [CrossRef]
35. Wu, W.; Xia, Z. Synthesis and color-tunable luminescence properties of Eu²⁺ and Mn²⁺-activated Ca₃Mg₃(PO₄)₄ phosphor for solid state lighting. *RSC Adv.* **2013**, *3*, 6051–6057. [CrossRef]
36. Ju, G.; Hu, Y.; Chen, L.; Wang, X.; Mu, Z. Blue persistent luminescence in Eu²⁺ doped Ca₃Mg₃(PO₄)₄. *Opt. Mater.* **2014**, *36*, 1183–1188. [CrossRef]
37. Nair, G.B.; Dhoble, S.J. White light emission through efficient energy transfer from Ce³⁺ to Dy³⁺ ions in Ca₃Mg₃(PO₄)₄ matrix aided by Li⁺ charge compensator. *J. Lumin.* **2017**, *192*, 1157–1166. [CrossRef]
38. Nair, G.B.; Dhoble, S.J. Orange light-emitting Ca₃Mg₃(PO₄)₄:Sm³⁺ phosphors. *Luminescence* **2017**, *32*, 125–128. [CrossRef]
39. Li, H.; Wang, Y. Effect of oxygen vacancies on the reduction of Eu³⁺ in Mg₃Ca₃(PO₄)₄ in air atmosphere. *Inorg. Chem.* **2017**, *56*, 10396–10403. [CrossRef]
40. Dickens, B.; Brown, W.E. The crystal structure of Ca₇Mg₉(Ca,Mg)₂(PO₄)₁₂. *Tscherm. Mineral. Petrogr. Mitt.* **1971**, *16*, 79–104. [CrossRef]
41. Steele, I.M.; Olsen, E. Crystal structure of natural stanfieldite from the Imilac pallasite. In Proceedings of the Lunar and Planetary Science Conference, Houston, TX, USA, 16–20 March 1992; pp. 1355–1356.
42. Brahın. Available online: <https://www.lpi.usra.edu/meteor/metbull.php?code=5130> (accessed on 27 April 2020).
43. Bondar, Y.V.; Perelygin, V.P. Fission track age of the Brahın pallasite. *Solar Syst. Res.* **2001**, *35*, 299–306. [CrossRef]

44. Rigaku Oxford Diffraction. *CrysAlisCCD, CrysAlisRED and CrysAlisPRO*; Oxford Diffraction Ltd.: Oxford, UK, 2017.
45. Sheldrick, G. *SHELXT*—Integrated space-group and crystal-structure determination. *Acta Crystallogr. A* **2015**, *71*, 3–8. [[CrossRef](#)]
46. Dolomanov, O.V.; Bourhis, L.J.; Gildea, R.J.; Howard, J.A.K.; Puschmann, H. Olex2: A complete structure solution, refinement and analysis program. *J. Appl. Crystallogr.* **2009**, *42*, 339–341. [[CrossRef](#)]
47. Britvin, S.N.; Dolivo-Dobrovolsky, D.V.; Krzhizhanovskaya, M.G. Software for processing the X-ray powder diffraction data obtained from the curved image plate detector of Rigaku RAXIS Rapid II diffractometer. *Zapiski Russ. Mineral. Soc.* **2017**, *146*, 104–107. (In Russian)
48. Brese, N.E.; O’Keeffe, M. Bond-valence parameters for solids. *Acta Crystallogr.* **1991**, *47*, 192–197. [[CrossRef](#)]
49. Moore, P.B. Bracelets and pinwheels: A topological-geometrical approach to the calcium orthosilicate and alkali sulfate structures. *Am. Mineral.* **1973**, *58*, 32–42.
50. Eysel, W. Crystal chemistry of the system $\text{Na}_2\text{SO}_4\text{--K}_2\text{SO}_4\text{--K}_2\text{CrO}_4\text{--Na}_2\text{CrO}_4$ and of the glaserite phase. *Am. Mineral.* **1973**, *58*, 736–747.
51. Gopal, R.; Calvo, C. Structural relationship of whitlockite and $\beta\text{-Ca}_3(\text{PO}_4)_2$. *Nat. Phys. Sci.* **1972**, *237*, 30–32. [[CrossRef](#)]
52. El Bali, B.; Boukhari, A.; Holt, E.M.; Aride, J. Calcium nickel orthophosphate: Crystal structure of $\text{Ca}_{8.5}\text{Ni}_{9.5}(\text{PO}_4)_{12}$. *Z. Kristallogr.* **1995**, *210*, 838–842.
53. Inorganic Crystal Structure Database ICSD. Available online: <https://icsd.fizkarlsruhe>. (accessed on 30 April 2020).



© 2020 by the authors. Licensee MDPI, Basel, Switzerland. This article is an open access article distributed under the terms and conditions of the Creative Commons Attribution (CC BY) license (<http://creativecommons.org/licenses/by/4.0/>).